Available online at www.sciencedirect.com
ScienceDirect
Trans. Nonferrous Met. Soc. China 34(2024) 724−736
Transactions of Nonferrous Metals Society of China
www.tnmsc.cn

First-principles study of stability of small vacancy clusters in aluminum

Tian-li SU, Xiang-shan KONG, Liang CHEN, Guo-qun ZHAO, Cun-sheng ZHANG

Key Laboratory for Liquid-Solid Structural Evolution and Processing of Materials, Ministry of Education, Shandong University, Jinan 250061, China

Received 12 August 2022; accepted 15 February 2023

Abstract: The vacancy cluster is one of the most common defects in aluminum alloys. Using density-functional theory-based first-principles calculations, the energetics of small vacancy clusters in aluminum, including voids, stacking fault tetrahedra (SFT), and vacancy platelets on the {111} plane, was investigated. It is found that the significant difference in monovacancy formation energies reported in literatures is mainly related to their used exchange-correlation functions. On average, LDA is the most reliable approximation for the monovacancy formation energies in Al, followed by PBE, PBEsol, PW91, and AM05. The results in this work confirm that the divacancy in Al is indeed energetically unfavorable. Moreover, vacancy clusters with a size smaller than five in any form are unstable against their corresponding number of isolated monovacancies. The SFT is the most stable form of most small vacancy clusters, followed by the void and vacancy platelet. These results are helpful to understand the experimentally observed size distributions of vacancy clusters in Al.

Key words: first-principles; Al; monovacancy; divacancy; vacancy clusters; stocking fault tetrahedra; vacancy platelet

1 Introduction

Aluminum (Al) alloys are widely used as constructive elements of automobiles, aircraft, and spacecraft due to their low density, lightweight, and good formability [1−3]. Vacancies are unavoidable and widespread defects in Al alloys during their synthesis process or in work conditions, such as the inert-gas condensation, electrodeposition, radiation, quenching, and serve plastic deformation. Vacancies can further aggregate to form voids, vacancy-type dislocation loops, and stacking fault tetrahedra (SFT), which would strongly affect the properties of Al alloys, especially the resistance to plastic deformation [4−6]. Therefore, the energetics and kinetics of vacancies and their clusters in Al have been investigated extensively using computational and experimental methods. However, there are still some incompleteness and controversy regarding the fundamental parameters of vacancies and their clusters.

Monovacancies are the simplest vacancy-type defects. Numerous first-principles works in the past two decades have systematically investigated the monovacancy properties in Al and predicted the formation energies of monovacancies at 0 K, however, which vary widely from 0.43 to 0.89 eV (see Table S1 in Supporting Materials for detailed literature data). This variation would significantly affect the prediction of the vacancy concentration in Al. On the other hand, the experimental monovacancy formation energy is 0.65−0.76 eV at high temperatures [7,8].

For the stability of the divacancy predicted by first-principles calculations, there are some controversies: stable or unstable relative to two isolated monovacancies. The early research [9,10],

Corresponding author: Xiang-shan KONG, Tel: +86-531-81696577, Fax: +86-531-88392811, E-mail: xskong@sdu.edu.cn;
Liang CHEN, Tel: +86-531-81696577, Fax: +86-531-88392811, E-mail: chenliang@sdu.edu.cn

DOI: 10.1016/S1003-6326(23)66430-1

using quantum mechanical density-functional theory (QMDFT), yielded that the first-nearest-neighbor (1nn) divacancy is unstable against two isolated monovacancies, while the second-nearest-neighbor (2nn) divacancy is barely energetically favorable with negligible binding energy. These first-principles results are completely contrary to the experimental view, where the 1nn divacancy is considered to be stable [11]. Before too long, this noticeable difference between the calculated and experimental results has been attributed to the use of small supercells in these early works. RADHAKRISHNAN and GAVINI [12] studied the effect of the supercell size on the vacancy cluster formation in Al using the orbital-free density-functional theory (OFDFT) and found that the divacancy binding energy changes sign from negative (repulsive interaction) for small supercell-sizes to positive (attractive interaction) for large supercell-sizes (>256 lattice sites). Further increasing the supercell, the divacancy binding energies change slightly (<0.05 eV). However, ZHANG et al [13] recently yielded an attraction of the divacancy with positive binding energies for the 1nn and 2nn divacancies, using the QMDFT in a small supercell with 108 lattice sites.

To date, three types of vacancy clusters, i.e., voids, vacancy-type dislocation loop, and SFT, have been observed in Al subjected to quenching, mechanical deformation, or ion irradiation. For many years, it was believed that SFT cannot appear in Al due to its high stacking fault energy, and this was supported by the calculations of vacancy clusters formation energy based on an elastic continuum expression [14]. It must be noted that the elastic theory cannot correctly yield the formation energy of small vacancy clusters. Then, the SFT was found to be the most stable structure of small vacancy clusters by molecular dynamics (MD) simulations with empirical interatomic potentials, followed by the vacancy platelet and voids [15]. However, the fidelity of the MD simulation seriously relies on the reliability of empirical interatomic potentials [16−19]. Therefore, it is necessary to use more precise first-principles calculations to study the stability of these three types of vacancy clusters. However, first-principles calculations of vacancy clusters in Al are rare. For the SFT, only WANG et al [20] predicted the stable configurations and binding energies of small SFTs containing 3−6 vacancies using QMDFT, where the pentavacancy was expected to play a crucial role in the process of vacancy clustering in Al due to its very high stability relative to other SFTs. For the vacancy-type dislocation loop, GAVINI et al [21] studied the energetics of planar vacancy clusters using OFDFT. They found that the planar quad-vacancy cluster energetically prefers to lie in the {111} plane and both the {111} quad-vacancy and 7-vacancy hexagonal vacancy clusters are stable with respect to the corresponding separated monovacancies. As far as we know, no energies and structures of small voids are reported by the first-principles calculations.

In this work, we firstly performed high-precision systematic QMDFT calculations for monovacancy and divacancy and try to resolve the controversies of the previous first-principles results. Then, we carried out a series of QMDFT calculations to provide accurate energies and structures of small vacancy clusters in Al, including voids, SFTs, and vacancy platelets on the {111} plane. Moreover, small vacancy clusters with vacancy number of 3−8 were considered due to the limitation of computation cost. Our calculations show that SFTs are the most stable vacancy clusters, followed by voids and vacancy platelets.

2 Methods

The supercell approach was used in the calculation of the vacancy cluster formation energies and binding energies. The formation energy per vacancy of the vacancy clusters ($E_{\mathrm{f}}^{V_n}$) is given by

$$E_{\mathrm{f}}^{V_n}=(E_{\mathrm{tot}}^{V_n}-\frac{N-n}{N}E_{\mathrm{tot}}^{\mathrm{bulk}})/n \tag{1}$$

where $E_{\mathrm{tot}}^{V_n}$ and $E_{\mathrm{tot}}^{\mathrm{bulk}}$ are the total energy of the supercell with the vacancy cluster V_n and without any defects, respectively, and n and N are the numbers of vacancies and lattice sites in the supercells, respectively. Specially, $E_{\mathrm{f}}^{V_1}$ denotes the monovacancy formation energy. The value of $E_{\mathrm{f}}^{V_{n>1}}<E_{\mathrm{f}}^{V_1}$ implies that the $V_{n>1}$ cluster is stable against n isolated monovacancies. The binding energy of the V_{n-1} cluster ($E_{\mathrm{b}}^{V_n}$) to the monovacancy can be calculated from the vacancy cluster formation energy, i.e.,

$$E_{\mathrm{b}}^{V_n}=E_{\mathrm{f}}^{V_1}+(n-1)E_{\mathrm{f}}^{V_{n-1}}-nE_{\mathrm{f}}^{V_n} \tag{2}$$

where the positive binding energy indicates an attractive interaction while a negative one means repulsion.

Since their focus is on mono- or divacancies, the majority of previous works used small supercells, containing 108 lattice sites or less. Here, to investigate the vacancy cluster, we used a few sets of large supercells, respectively, containing 108, 256, 500, and 1372 lattice points (i.e., 3×3×3, 4×4×4, 5×5×5, and 7×7×7 duplicates of a conventional FCC unit cell, respectively). All first-principles quantum mechanical calculations in the present work were carried out using the VASP simulation package with Blöchl's projector augmented wave (PAW) potential method [22−24]. The energy cutoff value of 400 eV was used for the plane-wave basis set, which is about 1.67 times higher than the VASP default largest energy for the Al element and larger than most previous first-principles works on the vacancy in Al. Five exchange-correlation functions were adopted, namely LDA [25], PW91[26], PBE [27], PBEsol [28], and AM05 [29]. Generally, the LDA is exact for a nearly homogeneous electron gas but would fail in systems with a large spatial variation in electron distribution. To incorporate effects due to inhomogeneous electron density, different flavors of GGA (generalized-gradient approximations) functions have been developed successively, such as PW91, PBE, and PBEsol. The PBEsol function is the optimized PBE to better describe equilibrium properties of densely packed solids and overcome the shortcomings of PBE function in describing surfaces. The AM05 function, including the surface effects like PBEsol, is expected to yield a better description of point defects than PBE and PW91. The real-space projection scheme was adopted due to these supercells with above 20 atoms. For the structural optimizations, the atomic positions, as well as the shape and size of the supercell, were allowed to change in the relaxation, unless specified. The convergence criterion for electronic self-consistency was set to be 1×10^{-6} eV, and the structural optimizations were truncated when the forces on each atom were less than 0.01 eV/Å.

The *k*-point convergence tests in previous works revealed that a mesh of 6912 *k*-point × atoms are sufficient to obtain a good convergence of the total energy within 0.002 eV/atom [30], and up to a mesh of 1×10^5 *k*-point × atoms is required to converge the monovacancy formation energy within 0.01 eV [31]. Here, we carefully tested the *k*-points convergence of not only the formation energies of the monovacancy but also the 1nn divacancy binding energies. For each calculation, irreducible *k*-points are generated by the Monkhorst−Pack scheme [22]. It can be seen from the results of the 3×3×3 supercell presented in Figs. 1(a) and (b) that the 5×5×5 *k*-point mesh, corresponding to 13500 *k*-point × atoms, is sufficient to obtain a good convergence of the monovacancy formation energy and 1nn divacancy binding energy less than 0.05 eV. When the supercell size increase from 3×3×3 to 4×4×4 FCC unit cells in the case of 5×5×5 *k*-point mesh, the monovacancy formation energy decreases 0.03−0.05 eV depending on the exchange-correlation functions, while the changes of the divacancy binding energies are negligible. Further tests in the 3×3×3 supercell with 5×5×5 *k*-point mesh reveal that difference between the smearing width of 0.2 and 0.1 eV can be negligible for the monovacancy formation energy and divacancy binding energy, respectively (see Figs. 1(c) and (d)). The change from the Methfessel−Paxton scheme to the tetrahedron method can respectively lead to 0.02−0.07 and 0.03−0.05 eV increase in the monovacancy formation energy and divacancy binding energy, depending on the exchange-correlation functions. In this work, the first-order Methfessel−Paxton scheme with a smearing width of 0.1 eV was used for the Fermi-surface smearing. Furthermore, it can be seen from these results that five exchange-correlation functions show very similar convergence behavior. Therefore, only PBEsol was adopted in further tests. For the 4×4×4 supercell, we checked the *k*-point convergence up to 186624 *k*-point×atoms, and found that 3×3×3 *k*-point mesh (6912 *k*-point×atoms) and the 5×5×5 *k*-point mesh (32000 *k*-point×atoms) are sufficient for the formation energy and binding energy, respectively. In addition, since the calculation cost is proportional to the cube of the number of atoms and the number of irreducible *k*-points, we only checked the cases of 3×3×3 *k*-point mesh in the 5×5×5 and 7×7×7 supercell, corresponding to 13500 and 37044 *k*-point×atoms, respectively. It is found that the 5×5×5 supercell with a 3×3×3 *k*-point mesh underestimates the monovacancy formation energy and overestimates the divacancy binding energy, while the 7×7×7 supercell with a

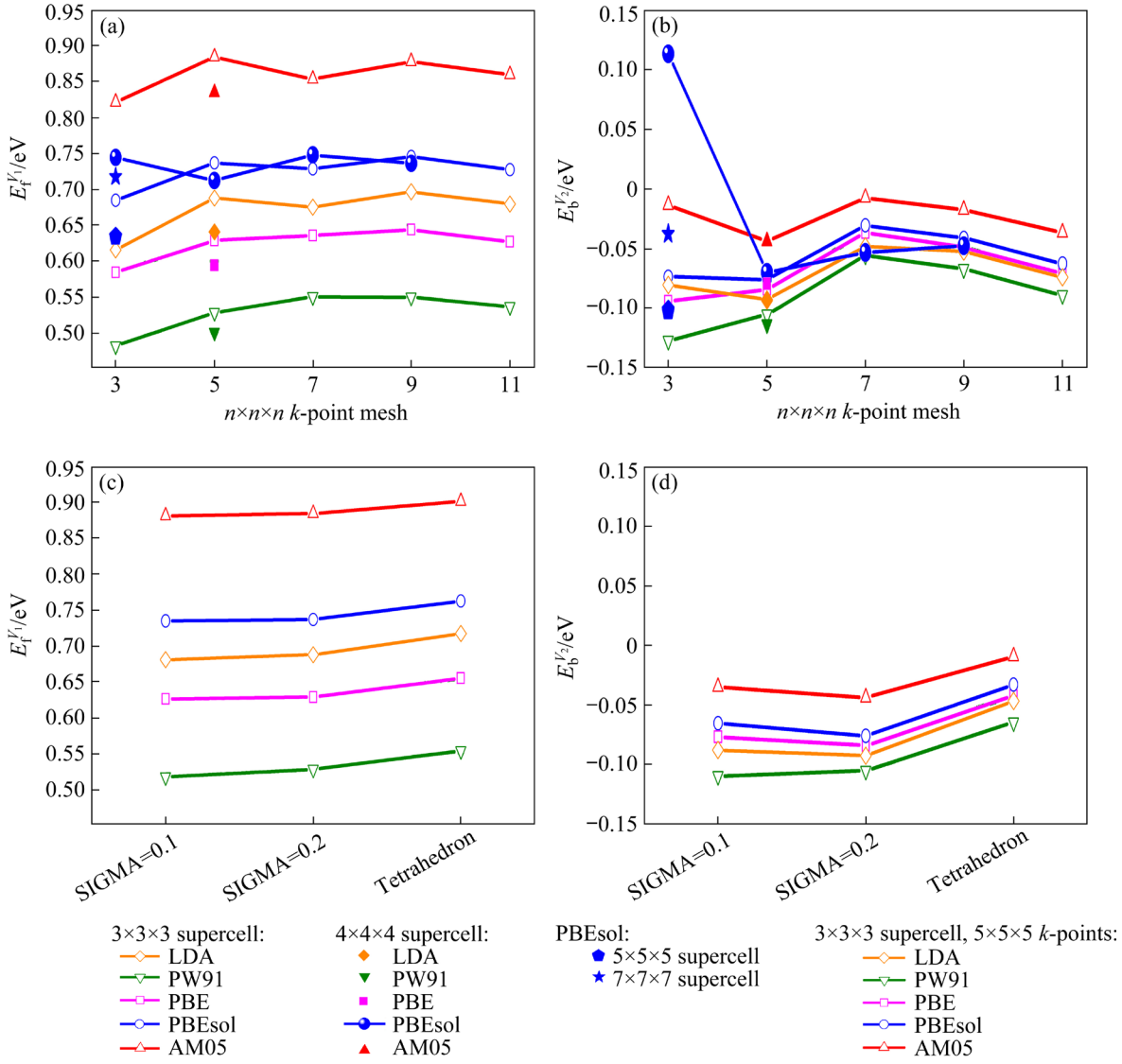

Fig. 1 Monovacancy formation energy (a) and 1nn divacancy binding energy (b) as function of $n\times n\times n$ k-point mesh; monovacancy formation energy (c) and 1nn divacancy binding energy (d) as function of electronic-states occupied schemes in 3×3×3 supercell with 5×5×5 k-point mesh

3×3×3 k-point mesh well converges compared to the case of 186624 k-point × atoms.

Note that, a large number of vacancy cluster configurations with a lower symmetry needed to be considered here, which would involve too many irreducible k-points for the calculations. Therefore, for computational efficiency reasons, the 3×3×3 supercell with 5×5×5 k-point mesh was adopted in the relaxation of numerous candidate configurations of the vacancy cluster, and the 4×4×4 supercell with 5×5×5 k-point mesh was used to obtain more precise results of the formation and binding energies of the most stable vacancy cluster detected. Moreover, the 5×5×5 and 7×7×7 supercells with 3×3×3 k-point mesh were adopted for checking and improving some results. According to the above convergence tests, this calculation process can be expected to obtain relatively reliable formation energies and binding energies of the vacancy clusters in Al. It should be mentioned that both supercells and k-point × atoms mesh used here are larger than those in most previous studies of the monovacancy formation energies in Al by the electronic-structure calculations.

3 Results and discussion

3.1 Basic properties

Figure 2 presents the lattice constants, bulk modulus, and cohesive energies, calculated here and

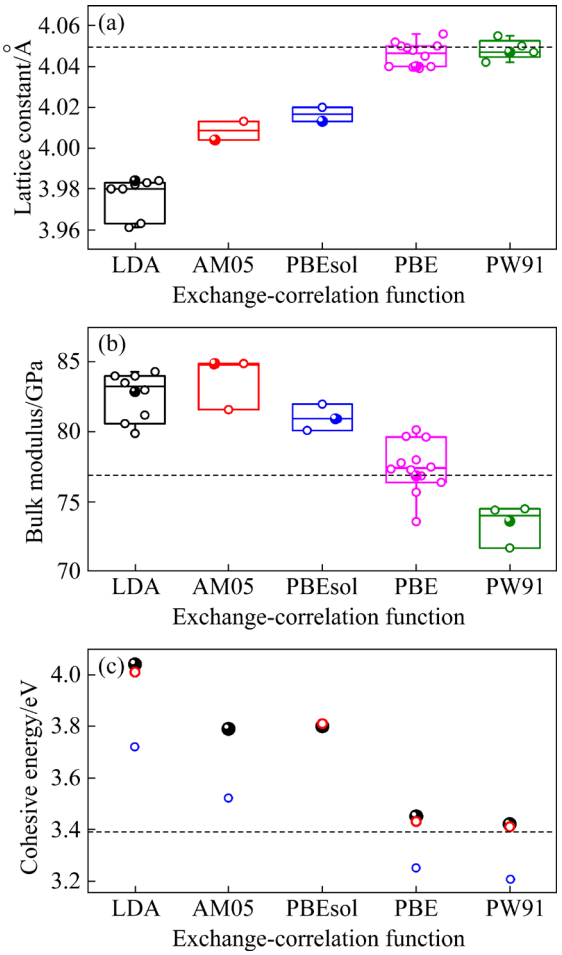

Fig. 2 Lattice constant (a), bulk modulus (b), and cohesive energy (c) of FCC Al at 0 K, distributed using standard boxplot, with 4×4×4 supercell and 5×5×5 *k*-point mesh used in calculations (The hollow and solid symbols represent the results reported in the literature and calculated in this work, respectively, see Tables S2−S4 in Supporting Materials for detailed literature data. Dash-dot lines denote the experimental results)

reported in the literature, which are classified by exchange-correlation functions. It can be seen that the exchange-correlation functions have a significant influence on these basic properties. When using the same functions, our calculated results are consistent with most of reported results. The slight difference results from the use of different simulation packages and calculation parameters, including cutoff energy, *k*-point mesh, supercell size, and so on. Therein PBE yields the best description of these basic properties, overall, followed by PW91, PBEsol, AM05, and LDA. Specifically, PW91 can well describe the lattice constant and the cohesive energy, like PBE, but its performance in predicting bulk modulus is underestimated by an average of 3.8%. Due to the well-known overbinding of the LDA function, it produces an underestimation of the lattice constant by an average of 1.2% and an overestimation of the bulk modulus and cohesive energy by an average of 8.5% and 19.5%, respectively. PBEsol and AM05 have a similar performance as the LDA function in describing these bulk parameters, only slightly better.

3.2 Formation energy of monovacancy

Figure 3(a) shows the monovacancy formation energies reported in the literature. Similar to the

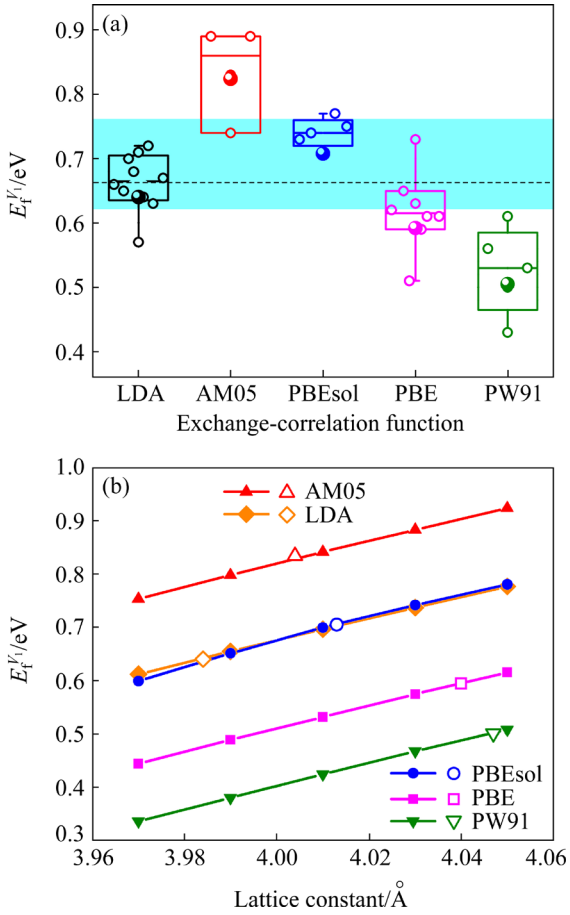

Fig. 3 Monovacancy formation energies distributed using standard boxplot reported in literature (hollow symbols, see Table S1 in Supporting Materials for detailed literature data) and calculated in this work (solid symbols, in 4×4×4 supercell with 5×5×5 *k*-point mesh) (The experimental monovacancy formation energies vary from 0.62 to 0.72 eV, marked by the cyan area; the dashed line denotes the revised monovacancy formation energy at 0 K using the experimental data [31]) (a); Monovacancy formation energies as function of lattice constant, marked by solid symbols and at equilibrium lattice constant, denoted by hollow symbols (b)

basic properties, when using the same exchange-correlation functions, most of the data differ within 0.1 eV, suggesting that the exchange-correlation function is the main reason for the large discrepancy in the reported monovacancy formation energies. The slight difference between these $E_{\mathrm{f}}^{V_1}$ data using the same exchange-correlation function results from different calculation parameters used, such as *k*-point mesh, supercell size, and the schemes of the Fermi-surface smearing, as shown in Fig. 1. Besides, the differences in the lattice constants used in these works may be another important factor for the monovacancy formation energies differences, which have been found to be very sensitive to the lattice constant in other metals [32]. As can be seen in Fig. 3(b), the monovacancy formation energy shows a linear dependence on the lattice constant, and the dependence is not sensitive to the choice of the exchange-correlation functional. An 0.01 Å increase in the lattice constant can lead to a 0.02 eV increase in the monovacancy formation energy. It can be seen from Fig. 2(a) that the variation of the lattice constant is in the range of 0.01−0.02 Å for the same exchange-correlation functions, which can induce 0.02−0.04 eV difference in the monovacancy formation energies. Because it would take too much space to consider each past calculation point by point, and the systematic error of the first-principles calculations limits the accuracy of both the present and past data, we are going to discuss the influence of the exchange-correlation functions on the monovacancy formation energy using the median of the data obtained by the same exchange-correlation functions. The data in this work, calculated by the 4×4×4 supercell with the 5×5×5 *k*-point mesh, are about 0.02 eV smaller than their corresponding median value.

The experiment data of the monovacancy formation energies can be used as the benchmark for the computed values; however, they are quite scattered, ranging from 0.62 to 0.76 eV. Moreover, it is difficult to make a direct and conclusive comparison between the experimental and computed values due to their large temperature differences, where the experimental measurements are limited to the temperature range of 60%−100% of the melting point while the first-principles calculations are generally performed at 0 K. It is very computationally expensive to account for temperature effects on the first-principles calculations. Recently, GLENSK et al [31] studied the temperature dependence of the Gibbs energy of vacancy formation in Al and gave a revised monovacancy formation energy at 0 K using the experimental data, that is, 0.66 eV. Here, we took the 0.66 eV as the benchmark to evaluate the reliability of exchange-correlation approximations in calculations on the vacancies in Al.

As shown in Fig. 3(a), the medians of these computed data are about 0.66, 0.86, 0.74, 0.62, and 0.53 eV for LDA, AM05, PBEsol, PBE, and PW91, respectively, differing significantly. AM05 yields the highest monovacancy formation energies, followed by PBEsol, LDA, PBE, and PW91. The difference between AM05 and PW91 is up to 0.33 eV. LDA gives the best monovacancy formation energy compared to experimental values. Similar results have been found in previous works about the monovacancy in metals [33]. This can be attributed to the well-known error cancellation effect: LDA largely overestimates the exchange energy of a free metal surface but underestimates by approximately the same magnitude the correlation energy. PBE slightly underestimates the monovacancy formation energy by 6%. This is because PBE underestimates the exchange surface energy but only slightly overestimates the correlation surface energy. Similar to PBE, PW91 also underestimates the monovacancy formation energy but with a larger error of up to about 20%. PBEsol, as a redesigned PBE with the aim to remedy the deficiencies of PBE for surfaces, however, did not yield a greatly better description of the monovacancy formation energies than the PBE, overestimating the monovacancy formation energy by about 12%. AM05, surprisingly, produces an unexpectedly large overestimation error (about 30%), which includes the surface effects and has been supposed to perform well for systems with an electronic surface. Similar conclusions can be drawn from our calculated data, except that PBEsol slightly outperforms PBE.

3.3 Binding energy of divacancy

We performed a series of systematic calculations about the 1nn and 2nn divacancy binding energies. Strikingly, the 1nn and 2nn divacancy binding energies are 0.12 and 0.05 eV, respectively, in the case of 4×4×4 supercell with

3×3×3 *k*-point mesh (6912 *k*-point × atoms), meaning an attractive interaction between two monovacancies. Moreover, the 1nn $E_b^{V_2}$ is very close to the experimental value (0.17 eV). Regrettably, the values of $E_b^{V_2}$ are always negative in other cases considered here, particularly for the cases with larger supercell and denser *k*-point mesh, indicative of a repulsive interaction. As shown in Figs. 4(a) and (b), up to 87808 *k*-point × atoms are required to obtain a very good convergence of the divacancy binding energies less than 0.01 eV. The 1nn and 2nn $E_b^{V_2}$ converge at 0 and −0.05 eV, respectively. Therefore, we believe that the calculated value of 0.12 eV is not true although it happens to be consistent with the experiment. Similarly, the attraction of the divacancy reported by ZHANG et al [13] may be due to the use of insufficient *k*-point × atoms (6912 *k*-point × atoms used in their work). In addition, the 23328 *k*-point×atoms, used in the early works [10], give converged values less than 0.05 eV for the 1nn and 2nn divacancies binding energies. We further checked the effect of supercell size on the divacancy binding energies. As can be seen in Fig. 4(a), the divacancy binding energies are negative for large supercell sizes (>256 lattice sites), in the range from −0.1 to 0 eV, meaning a repulsive interaction. Particularly, both 1nn and 2nn divacancy binding energies are negative in the case of 7×7×7 supercell containing 1372 lattice sites. This differs from the results of RADHAKRISHNAN and GAVINI [12] obtained by the coarse-graining OFDFT. It should be pointed out that the coarse-graining scheme of the OFDFT generally loses computational accuracy. In addition, as shown in Fig. 4(c), the effect of the lattice constant on both 1nn and 2nn $E_b^{V_2}$ is negligible. According to these calculated results, it can be concluded that the 1nn divacancy in Al is indeed unstable while the 2nn divacancy is barely energetically favorable.

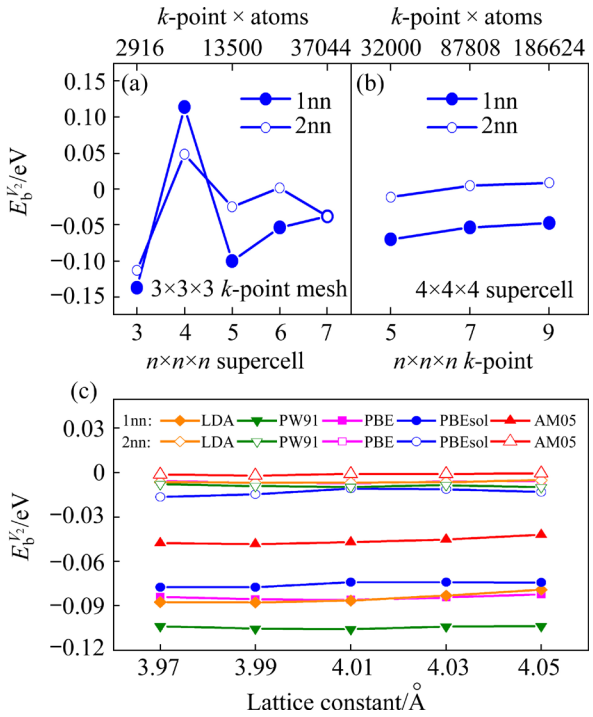

Fig. 4 Divacancy binding energies as functions of *n*×*n*×*n* supercell with 3×3×3 *k*-point mesh (a), *n*×*n*×*n* *k*-point in 4×4×4 supercell (b), and lattice constant (c) (The calculation setup for the results in (c) is the same as that of Fig. 3(b))

The noticeable difference between the calculated and experimental divacancy binding energies may result from the plausible explanation of the non-Arrhenius temperature dependence of vacancy concentration at high temperatures in experiments [31]. The formation energy of the monovacancy is generally considered to be a constant and thus the logarithm of the vacancy concentration varies linearly with the inverse temperature, i.e., an Arrhenius plot. However, for many metals, numerous experimental results show an upward curvature at high temperatures in the Arrhenius description of the vacancy concentration [8,34]. This curvature was explained by assuming contributions from defects other than monovacancies, namely divacancy, known as the monovacancy−divacancy model [34]. Thus, the binding energy of the divacancy was extracted from the vacancy concentration or self-diffusion coefficient based on the monovacancy−divacancy model. Although the monovacancy−divacancy model was commonly accepted in the past, it now may be implausible. In recent years, a series of high-precision first-principles calculations have revealed that the monovacancy formation energy is not constant but varies with temperature in metals, caused by the anharmonicity of the lattice vibrations [31,35,36]. Particularly, in Al, it has been confirmed that the temperature dependence of the monovacancy formation energy alone can well interpret the non-Arrhenius natures of the vacancy concentration observed in experiments [31], thus eliminating the need to introduce the divacancy in analyzing experimental data.

The anharmonicity of the lattice vibrations can also affect the divacancy binding energy. It has been reported by CARLING et al [9] that the anharmonicity makes the divacancy more unstable whereas the vibration entropy contributions slightly stabilize the divacancy, consequently, the divacancy binding energy at the melting temperature is still negative, that is, the divacancy is energetically unstable against two isolated monovacancies. In addition, the divacancy binding energy is also influenced by the configurational entropy. Recently, CAO et al [37] proposed a calculation procedure to evaluate the contribution of configurational entropy to the binding energy between two solute pairs. Here, we adopt a similar calculation procedure: the number of configurations of the 2N site system with a divacancy is $\Omega_{V_2}=2N^2$, and that of the 2N site with two isolated vacancies is $\Omega_{2V}=24N$, thus the contribution of the configurational entropy to the divacancy binding energy is

$$T\Delta S=k_{\mathrm{B}}T\left(\ln\,\Omega_{2V}-\ln\,\Omega_{V_2}\right)=k_{\mathrm{B}}T\ln\frac{N}{12} \tag{3}$$

where T is the temperature, ΔS is the entropy change, k_{B} is the Boltzmann constant, and N=108 or 256 adopted in our calculation. According to Eq. (3), the configurational entropy ($T\Delta S$) decreases monotonically with increasing temperature. Furthermore, the contribution of configurational entropy is always negative, which weakens the divacancy attraction. The configurational entropy effect also makes the binding of divacancy unstable.

Based on the above discussion, the theoretical calculation value of the binding energy of divacancy is negative, which is different from the experimental measurement. The results of these theoretical calculations were derived partly from the QMDFT calculations in small supercells (less than 100 atoms) with 4×4×4 k-point mesh and partly from the molecular-dynamics simulations using an interatomic potential with parameters determined from DFT calculations due to the very time-consuming high-precision QMDFT calculations of the anharmonic effect. And the simplicity of this calculation comes at the expense of the accuracy of the results. In addition to the above calculation factors such as lattice vibration and configuration entropy, impurities [38] also affect the divacancy binding energy measured in the experiments. Due to the influence of many factors, the discrepancy between theoretical calculations and experimental measurements is an open question.

3.4 Small vacancy clusters

Three different types of vacancy clusters are considered, namely, voids, SFT, and vacancy platelets on the {111} plane. To compare the relative stability of these three types of vacancy clusters, it is needed to find the lowest energy configurations for each vacancy cluster. However, as size increases, the number of vacancy cluster configurations increases dramatically, and it is very time-consuming computationally to find the lowest energy configuration for large vacancy clusters. In this work, due to the limitation of computation cost, only small vacancy clusters with n=3−8 were considered. For each type of vacancy cluster, a series of potential V_n configurations (more than 20 for V_{6-8}) were studied using the 3×3×3 supercell with the 5×5×5 k-point mesh, and then the configurations with lower energy were further checked using the 4×4×4 supercell with the 5×5×5 k-point mesh. Moreover, we also conducted a literature survey on atomic simulation studies of vacancy clusters in other FCC metals to cross-check our results. These calculations were done using PBEsol, and the most stable configuration was used to calculate the formation energy per vacancy and the binding energy. In addition, the most stable configurations for the voids were recalculated using LDA, PW91, PBE, and AM05 to evaluate the effect of the exchange-correlation functions.

Figure 5 shows the lowest energy configurations for the voids V_{3-8} and their corresponding formation energy per vacancy and binding energy. As for the cases of the above-mentioned mono- and di-vacancy, the formation energies per vacancy of the void obtained by different exchange-correlation functions differ greatly from each other, and AM05 yields the highest values, followed by PBEsol, LDA, PBE, and PW91. Moreover, AM05 predicts the strongest attraction between the vacancy cluster and monovacancy, PW91 gives the weakest attraction, while the binding energies yielded by LDA, PBE, and PBEsol are very close to each other. However, it can be seen from Figs. 5(b) and (c) that these five exchange-correlation functions predict similar trends for the formation energy per vacancy (binding energy) as a function of the vacancy number. Overall, the formation energy per vacancy shows a

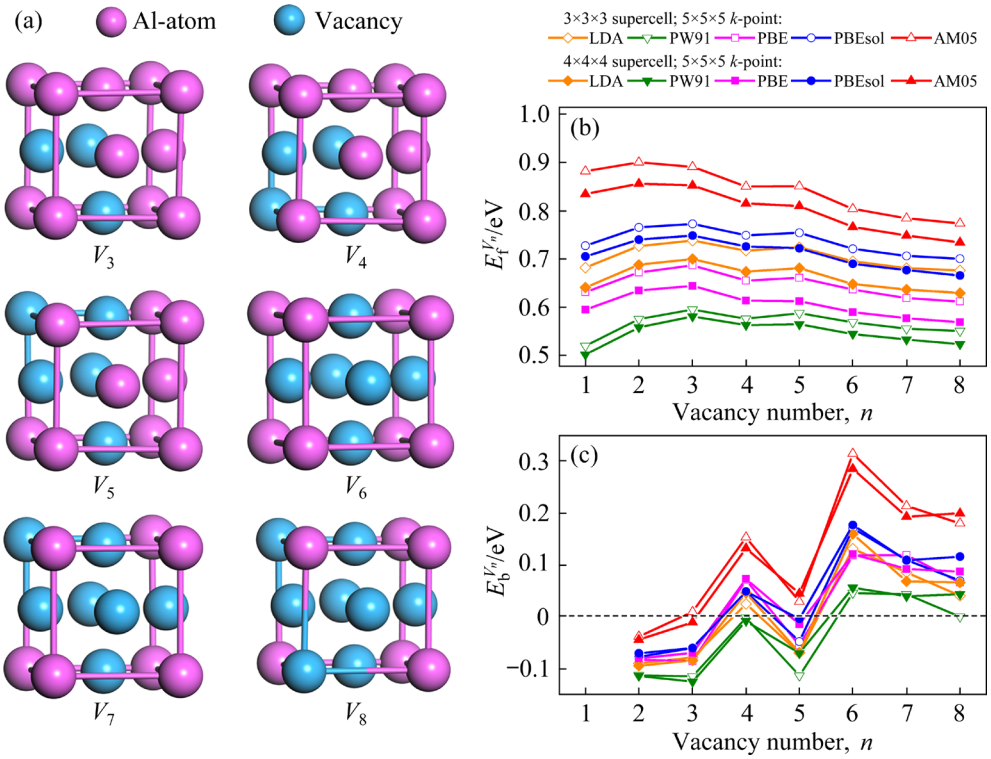

Fig. 5 Schematic configurations of the most stable V_{3-8} voids (a), and their corresponding formation energy per vacancy (b) and binding energy (c)

trend of increasing first and then decreasing with the vacancy number increase and finally becomes smaller than the monovacancy formation energy at a certain size, meaning that large voids are energetically favorable than their respective isolated monovacancies. Moreover, as the size increases, the binding energy starts out negative and then changes its sign to positive, suggesting that the interaction of the voids with the monovacancy shifts from repulsive to attractive. These results suggest that the voids would grow by capturing the isolated monovacancy and become more and more energetically stable. Moreover, as can be seen in Fig. 5(b), the differences between these exchange-correlation functions gradually decrease with increasing vacancy numbers. For example, the difference between the formation energies per vacancy obtained by AM05 and PW91 gradually narrows from 0.33 eV at V_1 to 0.23 eV at V_8.

For the case of the SFT, as shown in Fig. 6, the formation energy per vacancy is initially larger and then smaller than the monovacancy formation energy, taking n=4 as a boundary. This suggests that the SFT V_n changes from energetically unstable to stable against the n isolated monovacancies at n>4. Same to WANG et al [20], the V_5 SFT is also found to have the lowest formation energy per vacancy among all SFTs investigated in this work. The stable V_5 SFT consists of six vacancies and one aluminum atom, of which six vacancies are located in the face-centered positions of the unit cell, forming an octahedron, and the Al atom is located at the body-centered position of the unit cell, constituting a local body-centered cubic structure with its nearest-neighboring Al atoms. Furthermore, the formation energy per vacancy of V_5 is, respectively, much and slightly smaller than that of V_4 and V_6. This leads to a strong peak of the binding energy of the monovacancy to the SFT at n=5. As can be seen in Fig. 6, the binding energies of the V_1 to the V_4 and V_5 SFTs are 0.62 and −0.07 eV, respectively, meaning a very strong attraction of V_4 SFT to V_1 and a weak repulsion of V_5 SFT to V_1. This indicates that the V_5 SFT is particularly stable with a low inclination to grow or shrink. The binding energy of the V_1 to V_4 SFT is in fact much larger than other SFTs considered here, which are generally close to zero or negative, meaning very weak attraction or repulsion between these SFTs with V_1. Therefore, V_5 SFT can be expected as a

crucial nucleus for larger SFTs during the annealing of quenched supersaturated pure Al samples. The V_6 SFT corresponds to a perfect SFT. In addition, our predicted most stable configurations of $V_{3–6}$ and their corresponding binding energies agree well with the results of WANG et al [20].

Figure 7 shows the lowest energy configurations for the $V_{3–8}$ platelets on the {111} plane and their corresponding formation energy per vacancy and binding energy. When a vacancy number is a magic number, the vacancy platelet's structure is definitive, such as equilateral triangular shapes for V_3 and V_6 platelets and the perfect hexagonal shape for V_7 platelets. For non-magic vacancy number platelets, the additional vacancies are energetically favorable to be located at the edge center outside the magic number vacancy platelets and form a rhombus-shape with its nearest four vacancies in the vacancy platelet. Similar results have also been found in Ni. However, unlike the case in Ni [39], all vacancy platelets considered here in Al are energetically unfavorable relative to their corresponding n isolated monovacancies and are difficult to capture the isolated monovacancy. As can be seen in Figs. 7(b) and (c), the formation energies per vacancy of $V_{3–8}$ platelets are larger than the monovacancy

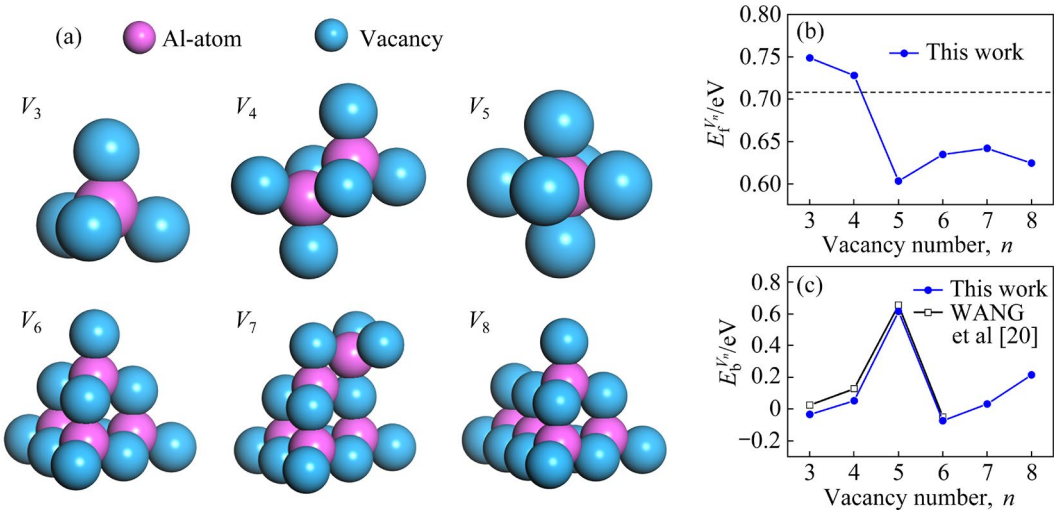

Fig. 6 Schematic configurations of the most stable $V_{3–8}$ SFTs (a), and their corresponding formation energy per vacancy (b) and binding energy (c) (These results were calculated in the case of a 4×4×4 supercell with a 5×5×5 k-point mesh. The dash line in (b) represents the monovacancy formation energy)

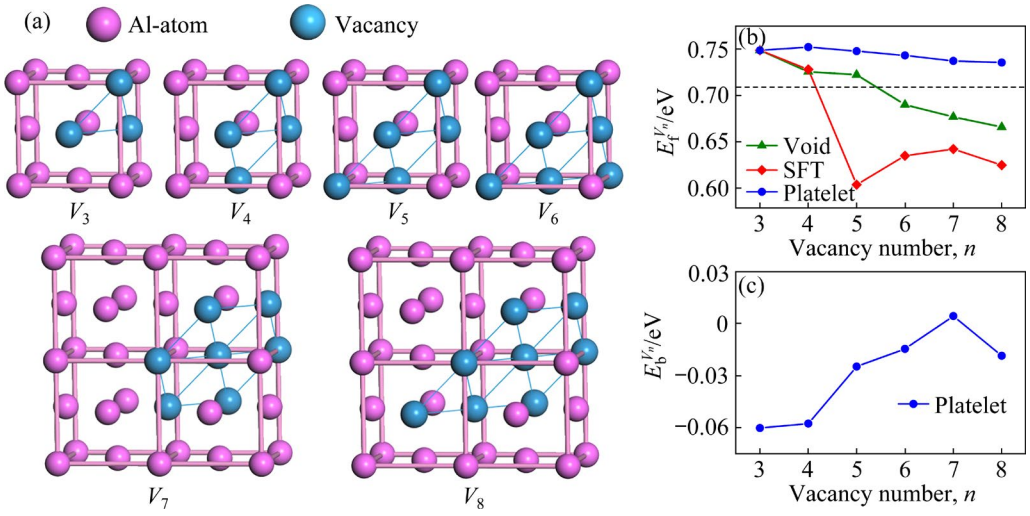

Fig. 7 Schematic configurations of the most stable $V_{3–8}$ platelets on {111} plane (a) and their corresponding formation energy per vacancy (b) and binding energy (c) (These results were calculated in the case of a 4×4×4 supercell with a 5×5×5 k-point mesh. The dash line in (b) represents the monovacancy formation energy)

formation energy and their binding energies to the additional monovacancy are most negative except for that of V_7 platelet, which is close to 0 eV. In addition, our results obtained by QMDFT are different from the previous results by OFDFT, where the {111} plane vacancy cluster is stable. This is the same as the above case of divacancies. These show that the coarse-graining scheme of the OFDFT proposed by RADHAKRISHNAN and GAVINI [12] may overestimate the binding between vacancies.

To compare the relative stability of the void, SFT, and platelet, the formation energies per vacancy of the most stable voids and SFTs obtained by PBEsol are replotted in Fig. 7(b). When n=3, their formation energies per vacancy are very close to each other, with a difference of less than 0.0002 eV. Therefore, it can be considered that the trivacancy has two stable configurations, i.e., a triangular of 1nn vacancies on the {111} plane and a body-centered tetrahedron configuration (a tetrahedron of 1nn vacancies with one Al atom at the center, known as Damask−Dienes−Weizer (DDW) [40] structure, see Fig. 6(a)). When n=4, the formation energies per vacancy of the void and SFT are very close and smaller than that of the platelet. The most stable structures of tetravacancies for the void and SFT types are the tetrahedron configuration consisting of four 1nn vacancies (see Fig. 5(a)) and two DDW structures with a common 1/2⟨110⟩ edge (see Fig. 6(a)), respectively. However, for $V_{n<4}$ clusters, all formation energies per vacancy are larger than the monovacancy formation energy, and their binding energies with the monovacancy are negative or positive close to zero. These indicate that the vacancies tend to remain as separated monovacancies as opposed to attracting and forming $V_{n<4}$ clusters. Thus, these $V_{n<4}$ clusters are difficult to serve as efficient nucleation sites for large vacancy clusters.

The stable V_n clusters begin to exist at n=5 and 6 in the form of SFT and void, respectively, and their stability is improved as the size increases. Moreover, among the $V_{n>4}$ clusters considered here, the SFT always has the lowest formation energy per vacancy, especially V_5 SFT, followed by the void and platelet, suggesting that the SFT is more stable than the void and platelet. The formation energies per vacancy of voids and {111} plane vacancy platelets decrease monotonically with the increase of size, while those of SFT do not change monotonically but fluctuately. Therefore, their relative stabilities would be changed for large clusters. This may be the reason why the SFT plays a dominant role in small-sized vacancy-type defects, while vacancy dislocation loops or voids dominate in large-sized vacancy-type defects, as observed in typical experiments [41]. The relative stability of large voids, SFT, and vacancy-type dislocation loops in Al requires further examination.

4 Conclusions

(1) The exchange-correlation functions are the main source of the large difference in the monovacancy formation energy reported in the previous literatures. Compared with the experimental results, LDA yields the best monovacancy formation energy, followed by PBEsol, PBE, AM05, and PW91. Our results confirm that the 1nn divacancy in Al is indeed unstable while the 2nn divacancy is barely energetically favorable at 0 K.

(2) The monovacancy formation energy shows a linear dependence on the lattice constant, while the lattice constant variation has little effect on the divacancy binding energy.

(3) The $V_{n<4}$ clusters in any form are unstable against their corresponding n isolated monovacancies, and the stable V_n clusters begin to exist at n=5 for SFTs and n=6 for voids; while all platelets on the {111} plane considered in this work are unstable. For most cases, the SFT is the most stable form of these small vacancy clusters, followed by the void and platelet. These results are helpful to understand the experimentally observed size distributions of vacancy clusters in Al.

CRediT authorship contribution statement

Tian-li SU: Conceptualization, Methodology, Investigation, Data curation, Formal analysis, Visualization, Writing − Original draft; **Xiang-shan KONG:** Conceptualization, Formal analysis, Validation, Funding acquisition, Writing − Original draft; **Liang CHEN:** Investigation, Conceptualization, Methodology, Funding acquisition, Writing − Review & editing; **Guo-qun ZHAO:** Supervision, Resources, Writing − Review & editing; **Cun-sheng ZHANG:** Writing − Review & editing.

Declaration of competing interest

The authors declare that they have no known competing financial interests or personal relationships that could have appeared to influence the work reported in this paper.

Acknowledgments

The authors would like to acknowledge the Key Research and Development Program of Shandong Province, China (No. 2021ZLGX01), the National Natural Science Foundation of China (No. 52071190), and the Shandong Provincial Natural Science Foundation, China (No. ZR2021YQ34).

Supporting Materials

Supporting Materials in this paper can be found at: http://tnmsc.csu.edu.cn/download/02-p0724-2022-0893-Supporting_Materials.pdf.

References

[1] JI Yuan-yuan, XU Yun-ze, ZHANG Bin-bin, BEHNAMIAN Y, XIA Da-hai, HU Wen-bin. Review of micro-scale and atomic-scale corrosion mechanisms of second phases in aluminum alloys [J]. Transactions of Nonferrous Metals Society of China, 2021, 31(11): 3205−3227.

[2] BAKHSHI R, FARSHIDI M H, SAJJADI S A. Strengthening of aluminium alloy 7005 through imposition of severe plastic deformation supplemented by different ageing treatments [J]. Transactions of Nonferrous Metals Society of China, 2021, 31(10): 2909−2921.

[3] WANG Yi-chang, WU Xiao-dong, YUE Lu, GUO Ming-xing, CAO Ling-fei. Aging precipitation behavior and properties of Al−Zn−Mg−Cu−Zr−Er alloy at different quenching rates [J]. Transactions of Nonferrous Metals Society of China, 2022, 32(4): 1070−1082.

[4] TAN Xiao-fen, WEYLAND M, CHEN Yu, WILLIAMS T, NAKASHIMA P N H, BOURGEOIS L. Growth of faceted, monolayer-coated nanovoids in aluminium [J]. Acta Materialia, 2021, 206: 116594.

[5] LIU Jian-qiu, HUANG Min-sheng, LI Zhen-huan, ZHAO Lv, ZHU Ya-xin. Microvoid growth mechanism in FCC polycrystals and a statistical damage model [J]. International Journal of Plasticity, 2020, 137: 102888.

[6] ZHAO Dong-dong, LOVVIK O M, MARTHINSEN K, LI Yan-jun. Twinnability of Al−Mg alloys: A first-principles interpretation [J]. Transactions of Nonferrous Metals Society of China, 2017, 27(6):1313−1318.

[7] SIMMONS R O, BALLUFFI R W. Measurements of equilibrium vacancy concentrations in aluminum [J]. Physical Review, 1960, 117(1): 52−61.

[8] TRIFTSHAUSER W. Positron trapping in solid and liquid metals [J]. Physical Review B, 1975, 12(11): 4634−4639.

[9] CARLING K M, WAHNSTROM G, MATTSSON T R, SANDBERG N, GRIMVALL G. Vacancy concentration in Al from combined first-principles and model potential calculations [J]. Physical Review B, 2003, 67(5): 054101.

[10] UESUGI T, KOHYAMA M, HIGASHI K. Ab initio study on divacancy binding energies in aluminum and magnesium [J]. Physical Review B, 2003, 68(18): 184103.

[11] DOYAMA M, KOEHLER J S. Quenching and annealing of zone-refined aluminum [J]. Physical Review, 1964, 134(2A): 522−529.

[12] RADHAKRISHNAN B, GAVINI V. Effect of cell size on the energetics of vacancies in aluminum studied via orbital-free density functional theory [J]. Physical Review B, 2010, 82(9): 094117.

[13] ZHANG Peng-bo, LI Yong-gang, ZHAO Ji-jun. Materials selection for nuclear applications in view of divacancy energies by comprehensive first-principles calculations [J]. Journal of Nuclear Materials, 2020, 538: 152253.

[14] ZINKLE S J, WOLFER W G, KULCINSKI G L, SEITZMAN L E. Stability of vacancy clusters in metals: II. Effect of oxygen and helium on void formation in metals [J]. Philosophical Magazine A, 1987, 55(1): 127−140.

[15] SHIMOMURA Y. Point defects and their clusters in f.c.c. metals studied by computer simulations [J]. Materials Chemistry and Physics, 1997, 50(2): 139−151.

[16] BONNY G, CASTIN N, TERENTYEV D. Interatomic potential for studying ageing under irradiation in stainless steels: the FeNiCr model alloy [J]. Modelling and Simulation in Materials Science and Engineering, 2013, 21(8): 085004.

[17] BONNY G, TERENTYEV D, PASIANOT R C, PONCE S, BAKAEV A. Interatomic potential to study plasticity in stainless steels: The FeNiCr model alloy [J]. Modelling and Simulation in Materials Science and Engineering, 2011, 19(8): 085008.

[18] ZHAO Shi-jun, VELISA G, XUE Hai-zhou, BEI Hong-bin, WEBER W J, ZHANG Yan-wen. Suppression of vacancy cluster growth in concentrated solid solution alloys [J]. Acta Materialia, 2017, 125: 231−237.

[19] OSETSKY Y N, SERRA A, VICTORIA M, GOLUBOV S I, PRIEGO V. Vacancy loops and stacking-fault tetrahedra in copper: I. Structure and properties studied by pair and many-body potentials [J]. Philosophical Magazine A, 1999, 79(9): 2259−2283.

[20] WANG Hao, RODNEY D, XU Dong-sheng, YANG Rui, VEYSSIERE P. Pentavacancy as the key nucleus for vacancy clustering in aluminum [J]. Physical Review B, 2011, 84(22): 220103.

[21] GAVINI V, BHATTACHARYA K, ORTIZ M. Vacancy clustering and prismatic dislocation loop formation in aluminum [J]. Physical Review B, 2007, 76(18): 180101.

[22] KRESSE G, FURTHMULLER J. Efficient iterative schemes for ab initio total-energy calculations using a plane-wave basis set [J]. Physical Review B, 1996, 54(16): 11169−11186.

[23] KRESSE G, HAFNER J. Ab initio molecular dynamics for liquid metals [J]. Physical Review B, 1993, 47(1): 558−561.

[24] BLOCHL P E. Projector augmented-wave method [J]. Physical Review B, 1994, 50(24): 17953−17979.

[25] PERDEW J P, ZUNGER A. Self-interaction correction to density-functional approximations for many-electron systems [J]. Physical Review B, 1981, 23(10): 5048−5079.

[26] PERDEW J P, CHEVARY J A, VOSKO S H, JACKSON K A, PEDERSON M R, SINGH D J, FIOLHAIS C. Atoms, molecules, solids, and surfaces: Applications of the generalized gradient approximation for exchange and correlation [J]. Physical Review B, 1992, 46(11): 6671−6687.
[27] PERDEW J P, BURKE K, ERNZERHOF M. Generalized gradient approximation made simple [J]. Physical Review Letters, 1996, 77(18): 3865−3868.
[28] PERDEW J P, RUZSINSZKY A, CSONKA G I, VYDROV O A, SCUSERIA G E, CONSTANTIN L A, ZHOU Xiao-lan, BURKE K. Restoring the density-gradient expansion for exchange in solids and surfaces [J]. Physical Review Letters, 2008, 100(13): 136406.
[29] ARMIENTO R, MATTSSON A E. Functional designed to include surface effects in self-consistent density functional theory [J]. Physical Review B, 2005, 72(8): 085108.
[30] NAZAROV R, HICKEL T, NEUGEBAUER J. Vacancy formation energies in fcc metals: Influence of exchange-correlation functionals and correction schemes [J]. Physical Review B, 2012, 85(14): 144118.
[31] GLENSK A, GRABOWSKI B, HICKEL T, NEUGEBAUER J. Breakdown of the Arrhenius law in describing vacancy formation energies: The importance of local anharmonicity revealed by ab initio thermodynamics [J]. Physical Review X, 2014, 4(1): 011018.
[32] HUANG Gui-yang, JUSLIN N, WIRTH B D. First-principles study of vacancy, interstitial, noble gas atom interstitial and vacancy clusters in bcc-W [J]. Computational Materials Science, 2016, 123: 121−130.
[33] DELCZEG L, DELCZEG-CZIRJAK E K, JOHANSSON B, VITOS L. Assessing common density functional approximations for the ab initio description of monovacancies in metals [J]. Physical Review B, 2009, 80(20): 205121.
[34] KRAFTMAKHER Y. Equilibrium vacancies and thermo-physical properties of metals [J]. Physics Reports, 1998, 299(2/3): 79−188.
[35] BOCHKAREV A S, van ROEKEGHEM A, MOSSA S, MINGO N. Anharmonic thermodynamics of vacancies using a neural network potential [J]. Physical Review Materials, 2019, 3(9): 093803.
[36] SMIRNOVA D, STARIKOV S, LEINES G D, LIANG Yan-yan, WANG Ning, POPOV M N, ABRIKOSOV I A, SANGIOVANNI D G, DRAUTZ R, MROVEC M. Atomistic description of self-diffusion in molybdenum: A comparative theoretical study of non-Arrhenius behavior [J]. Physical Review Materials, 2020, 4(1): 013605.
[37] CAO Shuo, ZHANG Shang-zhou, LIU Jian-rong, LI Shu-jun, SUN Tao, LI Jian-ping, GAO Yang, YANG Rui, HU Qing-miao. Interaction between Al and other alloying atoms in α-Ti for designing high temperature titanium alloy [J]. Computational Materials Science, 2021, 197: 110620.
[38] DONG Ming-ye, ZHAO Yue, LI Quan, WANG Fu-de, WU Ai-ping. Effects of Cd addition in welding wires on microstructure and mechanical property of wire and arc additively manufactured Al−Cu alloy [J]. Transactions of Nonferrous Metals Society of China, 2022, 32(3): 750−764.
[39] ZHAO Shi-jun, ZHANG Yan-wen, WEBER W J. Stability of vacancy-type defect clusters in Ni based on first-principles and molecular dynamics simulations [J]. Scripta Materialia, 2018, 145: 71−75.
[40] DAMASK A C, DIENES G J, WEIZER V G. Calculation of migration and binding energies of mono-, di-, and trivacancies in copper with the use of a morse function [J]. Physical Review, 1959, 113(3): 781−784.
[41] SATOH Y, YOSHIIE T, MORI H, KIRITANI M. Formation of stacking-fault tetrahedra in aluminum irradiated with high-energy particles at low-temperatures [J]. Physical Review B, 2004, 69(9): 094108.

铝中小空位团簇稳定性的第一性原理研究

苏恬莉，孔祥山，陈 良，赵国群，张存生

山东大学 材料液固结构演化与加工教育部重点实验室，济南 250061

摘 要：空位团簇是铝合金中最常见的缺陷之一。利用基于密度泛函理论的第一性原理计算，研究铝中孔洞、层错四面体(SFT)和{111}平面上的空位板等小空位团簇的能量学，发现文献报道的单空位形成能的显著差异主要与它们所使用的交换相关泛函数有关，LDA 是 Al 中单空位形成能最可靠的近似，其次是 PBE、PBEsol、PW91 和 AM05。本文结果证实 Al 中的双空位在能量上是不稳定的。此外，任何结构中小于 5 的空位团簇相对于相应数量的孤立单空位都是不稳定的。SFT 是大多数小空位团簇中最稳定的结构，其次是孔洞和空位板。这些结果有助于理解实验观测到的铝中空位团簇的尺寸分布。

关键词：第一性原理；铝；单空位；双空位；空位团簇；层错四面体；空位板

(Edited by Wei-ping CHEN)